Chemistry Europe
European Chemical Societies Publishing

Special Collection

Solvent-Controlled Intermolecular Proton-Transfer Follows an Irreversible Eigen-Weller Model from fs to ns

Alexander Grandjean,[a] J. Luis Pérez Lustres,*[b] and Gregor Jung*[a]

In memory of Prof. Dr. Markus Gerhards (Fachbereich Chemie, Technische Universität Kaiserslautern, Germany)

Intermolecular Proton Transfer (PT) dynamics can be best studied by optical spectroscopy, which can cover the vast timescale spanned by the process. PT in a hydrogen bonding complex between a pyranine-based photoacid and a trialkylphosphine oxide is addressed. The photoreaction is traced with the help of femtosecond transient absorption and picosecond-resolved fluorescence. Characteristic kinetics and spectra of the intervening species are isolated by global analysis and spectral decomposition of time-resolved fluorescence. It is found that the shared proton shifts towards the phosphine site upon photoexcitation in acetonitrile. The process occurs on the sub-picosecond timescale, essentially, under solvent control. Despite the ultrafast rate, an equilibrium between the complex and the hydrogen-bonded ion pair (HBIP) is established. Further reaction steps are delayed to the nanosecond timescale, where formation of the excited deprotonated form is observed. The far-reaching consistency between the various methods supports an irreversible Eigen-Weller mechanism in the excited state.

1. Introduction

Fluorescent photoacids become much more acidic upon optical excitation and constitute a mighty tool to study intermolecular proton transfer in the excited-state (ESPT). The latter process can be triggered by ultrafast laser excitation of a pre-established hydrogen-bonded pair between the photoacid and a base. Since optical properties change during deprotonation, the dynamics of all participating species can be monitored precisely by time-resolved fluorescence and transient absorption spectroscopy in the optical spectral region.

ESPT was first reported by Weber in 1931.[1] Later on, Förster introduced the so-called Förster-Cycle, which relates the proton transfer free energies in ground- and excited states to the transition energies of protonated and deprotonated forms.[2] A strong reduction of the pK_a value of the photoacid ROH upon optical excitation may induce ultrafast proton transfer to the solvent or to a basic species in the neighborhood, which is accompanied by strongly red-shifted emission of the deprotonated form RO^-. Eigen and Weller found experimental evidences for further reaction stages involving formation of an encounter complex and a contact ion pair just before and after the elementary proton transfer step.[3–7] The formation of these species was confirmed by ultrafast spectroscopy.[8–14] Proton transfer to solvent (PTTS) dynamics was found to be very complex. In 1988, Pines et al. addressed 8-hydroxypyrene-1,3,6-trisulfonic acid (HPTS, also called pyranine), which dissociates in water and alcohols on the picosecond timescale.[15] The process was monitored by picosecond-resolved fluorescence. The latter was explained by the diffusional motion of a proton in the proximity of an ion. Solution of the corresponding Debye-Smoluchowski-Equation (DSE) models picosecond PTTS dynamics successfully, suggesting that geminate proton recombination plays a major role in the photodissociation of strongly charged HPTS. Further experiments exposed apparent inconsistencies with the exact solution of the DSE.[16,17] The model was refined by introducing the solvent-separated ion pair (SSIP) as additional reaction intermediate. The SSIP is conjectured as a loosely bound complex of charged conjugated acid and base, which are separated by several solvent molecules. The hydrogen bonding interaction would be responsible for spectral differences between the hydrogen-bonded ion pair (HBIP) and the SSIP. The fully-separated ion pair (FSIP) is formed when the distance between the conjugated base and the proton becomes so large that Coulomb interactions vanish completely.[17–20]

The role of the solvent coordinate as promoter of the PTTS reaction has been emphasized in several studies,[21–23] where proton transfer from strong photoacids to accepting solvents was monitored at high time resolution. It was found that ultrafast proton transfer occurs in a non-equilibrated solvent environment. Consequently, dynamic spectral shifts of the

[a] A. Grandjean, Prof. Dr. G. Jung
Biophysikalische Chemie, Universität des Saarlandes, FR Chemie, Gebäude B2 2, Postfach 151150, D-66041 Saarbrücken (Germany)
E-mail: g.jung@mx.uni-saarland.de
[b] Dr. J. L. Pérez Lustres
Current Address: Fachbereich Physik, Freie Universität Berlin, Arnimallee 14, 14195 Berlin (Germany)
and
Experimental work conducted at former affiliation: Physikalisch Chemisches Institut, Universität Heidelberg, Im Neuenheimer Feld 229, D-69120 Heidelberg (Germany)
E-mail: perez.lustres@fu-berlin.de

Supporting information for this article is available on the WWW under https://doi.org/10.1002/cptc.202100177

An invited contribution to the "GDCh and ChemPhotoChem: 5-Year Anniversary" Special Collection

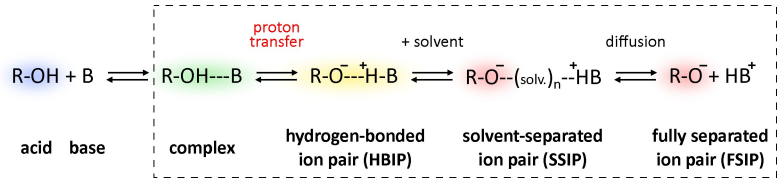

Scheme 1. Reaction stages in the Eigen-Weller Model. The dashed line contains the reaction steps addressed in this work.

involved species also contribute to the time-resolved fluorescence and transient absorption signals measured at single wavelengths. Therefore, corrections have to be applied to extract true PTTS population dynamics from the fluorescence and transient absorption signals. This uncovers a reaction mechanism in which the elementary proton transfer step is controlled by solvent dynamics, whereas slower proton ejection out of the solvent shell occurs exponentially in water and alcohols.[21,22] The mechanism applies in weaker acids too.[24] Considering all these studies, a most general five stage model is envisioned for the description of intermolecular proton transfer reactions (Scheme 1): the neat protonated acid (ROH), the encounter/reactive complex (CPX), the hydrogen-bonded ion pair (HBIP), the solvent-separated ion pair (SSIP) and the fully separated ion pair (FSIP) interconvert in a broad range of timescales in a consecutive manner. Strong spectral overlap, vastly different timescales and fleeting populations of many intermediates make PTTS experimentally challenging. The problem demands broadband detection methods with high time and spectral resolution.

The influence of the environment on the proton transfer reaction remains unclear. Much previous work concentrates on PTTS, where the roles of the solvent as proton acceptor and as the environment facilitating the proton transfer reaction can not be separated.[11,14–17,25] Acetate buffers were also employed,[8–10] but competition of acetate ion and water as proton acceptors complicates the analysis. A different strategy is here followed: optical excitation of a pre-established hydrogen-bonded complex between a photoacid and a base should trigger intermolecular proton transfer in a non-basic solvent. The approach was successfully applied by a number of groups,[19,26–29] demonstrating that such molecular systems are ideally suited to monitor intermolecular proton transfer dynamics. Under optimal conditions, optical spectra of the various intermediates can be determined by global analysis of fluorescence and transient absorption data. This also opens the way to analyze temperature dependencies and obtain characteristic activation parameters.

Ideally, proton-transfer complexes for intermolecular proton transfer must fulfill a series of requirements as high photostability and fluorescence quantum yield, high association constants in the ground state, single complexation sites, high spectral contrast between bound and unbound species and be electrically neutral to favor good solubility in a broad range of solvents. The molecular system presented in our previous publication[30] fulfills these conditions. A pyrene-based photoacid (ROH, with $pK_a = 4.7$ and $pK_a^* = -2.7$) binds a tri-n-octyl-phosphine oxide (TOPO) in the ground electronic state, see Scheme 2.[30,31] Excited-state proton transfer occurs along the hydrogen-bond of the complex. The fluorescence bandshapes of the involved species were isolated via steady-state spectroscopy and associated solvatochromic analysis. Here, complementary time-resolved work is presented. A combination of broadband ultrafast transient-absorption and time-resolved fluorescence spectroscopy at single wavelengths is applied. Reference spectra from steady-state spectroscopy help to expose the underlying proton transfer dynamics.

2. Results

Stationary spectroscopy of all species involved in the ROH:TOOPO proton transfer system was analyzed in Reference [30]. UV-Vis absorption spectra of ROH (maximum at 428 nm) and complex (441 nm) forms were measured directly in titration experiments. The UV-Vis spectrum of the deprotonated anionic form (564 nm) was measured in non-dried acetonitrile, where ROH dissociates in the presence of small amounts of water. Fluorescence spectra are, however, difficult to isolate, because of the proton transfer reaction occurring to various extents in different solvents. Thus, ROH emits with maximal intensity at 477 nm in extra-dry acetonitrile. Note that, in this work, fluorescence is analyzed in the form of stimulated emission (SE) cross-section. The latter is calculated by multiplying the spectrally corrected fluorescence quantum distribution over wavelengths by λ^4.[32] The deprotonated form shows very sharp emission centered at 572 nm in the same solvent, as determined by optical excitation of the deprotonated form in the ground state. However, the emission spectrum observed upon

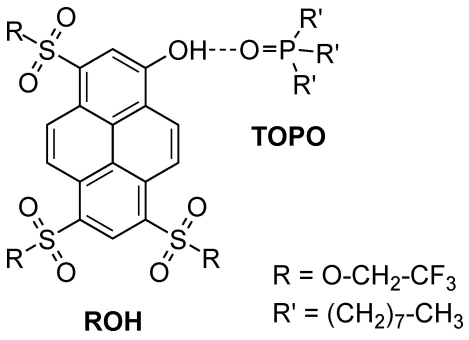

Scheme 2. Expected molecular structure of the hydrogen bonding complex between the pyrene photoacid (ROH) and the tri-n-octyl-phosphine oxide base (TOPO).

photoexcitation of the complex exhibits an involved solvent dependence. This behavior was interpreted, first, as the result of the proton transfer reaction in the excited state, the extent of which is solvent dependent. Thus, the emission spectrum is the sum of individual spectra of the hydrogen-bonded ROH:TOPO complex and the HBIP in a ratio given by the solvent polarity and acid-base properties. For polar solvents, as acetonitrile, emission of the deprotonated form is also detected (see Figure SI 3). Second, the spectral position of the individual forms depends on solvent polarity, too. These two manifestations of the solvent effect were modeled in Reference [30], where emission maxima of 505 and 547 nm were deduced for the complex and the HBIP forms, respectively, in acetonitrile. The so-deduced stationary species-associated optical spectra (SAS) are collected in Figure 1.

The transient absorption spectrum of ROH in acetonitrile shows a blue shift of the excited-state absorption (ESA) signal between 500 and 550 nm during the first 1 ps. The signal decays simultaneously on the blue edge of the stimulated emission band (SE) around 450 nm. This spectral evolution still continues in the 10 ps window but with much smaller amplitude, Figure 2. After that, the spectrum virtually stays and decays on the nanosecond timescale with constant shape (not shown).

Fluorescence decay was measured in the nanosecond timescale across the emission band in 10 nm steps by time-correlated single-photon counting (TCSPC). The fluorescence decay is non trivial: a three exponential function with an additional impulsive contribution is needed to fit the data globally, Figure 3. The impulsive contribution accounts for an ultrafast decay of the signal on the blue edge of the emission band, suggesting an unresolved spectral red-shift. Decay times τ_{1-2} of 0.62(9) ns and 2.1(2) ns show small overall amplitude ($< 10\%$). Remarkably, they show negative and positive contributions, respectively, on the blue flank of the fluorescence band, which suggests a reversible process of small amplitude (see Supporting Information, Figure SI 4). Finally, the main decay time is $\tau_3 = 4.31(1)$ ns and its amplitude resembles the spectral distribution of the stationary fluorescence spectrum.

The transient absorption of the hydrogen-bonded complex ROH:TOPO develops on a broad time range. In the picosecond timescale a red shifted SE band peaking initially at about 575 nm grows and blue shifts within 5 ps, see upper panel of Figure 4. Concomitantly, an ESA band narrows, blue-shifts and rises until it reaches its maximum at 470 nm by 5 ps delay. These spectral changes also affect the apparent bleach contribution on the blue side of our spectral window, which decays and blue shifts. The spectrum shows a distinct phase in the nanosecond timescale, where sharp isosbestic points suggest a state-to-state interconversion. This later phase of the excited-state dynamics is insufficiently resolved in the femtosecond transient absorption experiment.

The picosecond time-resolved fluorescence signal was measured across the fluorescence band of the ROH:TOPO complex in 10 nm steps, see Figure 5. This experiment addresses the slow dynamics just sensed in the femtosecond transient absorption discussed previously. It is important to

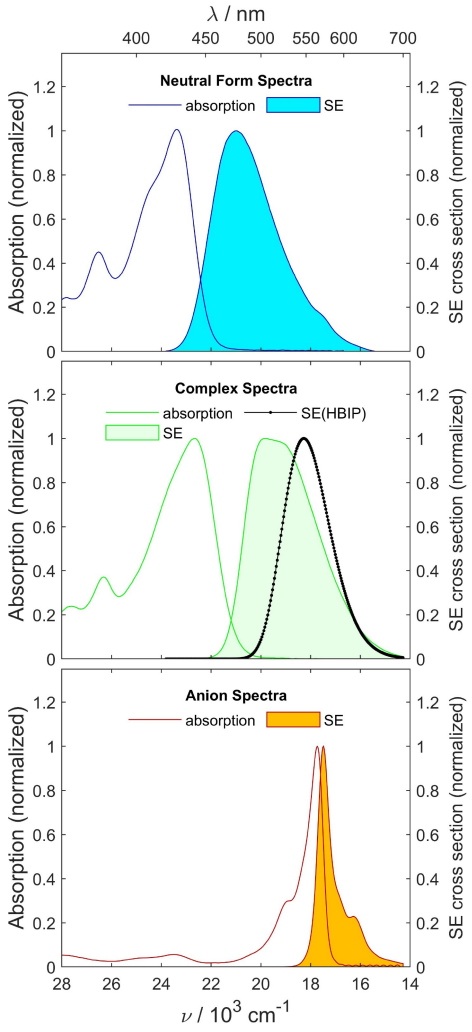

Figure 1. Stationary UV-Vis absorption and fluorescence spectra of the neutral (ROH, top panel) and deprotonated (anion RO^-, bottom panel) forms in acetonitrile, as determined experimentally. All fluorescence spectra were transformed into cross-section for SE. Emission spectra of the hydrogen-bonded ROH:TOPO complex and the hydrogen-bonded ion pair (HBIP) are also shown in the middle panel together with the corresponding absorption spectrum of the complex. Both were derived from a solvatochromic analysis of the fluorescence emission spectrum of ROH:TOPO in solvent mixtures as shown in reference [30]. Note, excitation of the complex results in a steady-state emission spectrum with contributions of all four shown species (see Figure SI 3), since ROH concentration is estimated to be 3% in the ground state. The composition of emission spectrum depends on the solvent properties. Spectra are color-coded as indicated by the corresponding legends in each panel.

note that, at the TOPO concentration of 30 mM, about 3% of the ground-state population still remains as free ROH. For the excited state, this ratio is further modulated by the excitation wavelength and the corresponding extinction coefficients of the two species. This means that ROH emission is expected to contribute significantly at wavelengths below 480 nm. Therefore, fourteen different wavelengths between 490 and 620 nm were fitted globally, in order to avoid contamination of proton transfer dynamics in the ROH:TOPO complex by residual emission of the free ROH form. A complex spectral dependence is observed. Three-exponential functions were used. An

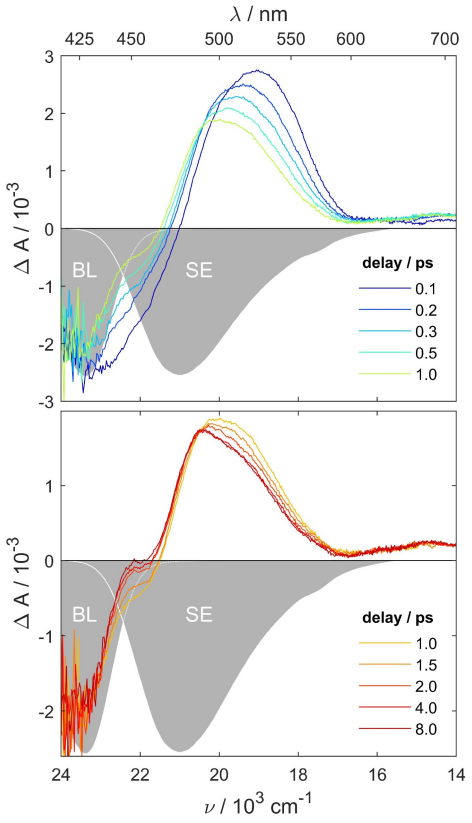

Figure 2. Transient absorption signal of the photoacid ROH measured in acetonitrile at magic angle polarization (λ_{exc} = 410 nm). The upper panel shows the evolution during the first 1 ps, while the lower panel addresses the next 8 ps. The time delays are indicated by the legend. Gray-filled areas show normalized negative absorption of the photoacid (BL) and its fluorescence bandshape converted to cross-section of stimulated emission (SE), as indicated by the labels.

impulsive component following the instrument response function in time was considered too. The spectral distributions of the three exponentials are summarized next, Figure 6. First, the impulsive component is consistent with an spectral broadening occurring at earliest time. Next, between impulsive and ns stages, an intermediate small-amplitude time constant τ_1 of 0.58(3) ns is deduced. Finally, decay components τ_{2-3} of 4.65(2) ns and 6.09(6) ns were determined. The corresponding spectral amplitudes, the DAS, are shown in Figure 6. Remarkably, τ_3 matches the decay time of the deprotonated form in pure acetonitrile: 6.15 ns.[30] Furthermore, its associated amplitude matches the SE bandshape of RO^-, indicating that the latter is formed non-reversibly in the excited-state.

The time-resolved fluorescence signal of the ROH:TOPO complex was analyzed separately in the range between 440 and 480 nm. As stated above, residual emission of free ROH is expected here (Figures SI 3, 7 and 14). This spectral area overlaps the absorption spectrum of the complex too (see Figure 1, middle panel). Five wavelengths were fitted globally (Figures SI 5 and 6). This results in decay times τ_{1-2} of 3.3(1) and 4.56(4) ns. Remarkably, the decay times and the spectral distribution (see Figure SI 6) resemble those deduced for the ROH form in acetonitrile (Figure SI 4), suggesting that emission at wavelengths shorter than 490 nm stems mostly from the free ROH form. In support, the normalized χ^2 values obtained for the global fits increase slightly at around 490 nm, where an approximate border between the blue emitting free ROH form and the red-shifted ROH:TOPO complex emission may be traced. See section 7 of the Supporting Information for further details.

Summarizing, complexation with TOPO induces prominent spectral dynamics spanning the femtosecond to nanosecond timescale, as observed by broadband femtosecond transient absorption spectroscopy. The signature of the RO^- form is identified clearly at late times but slow dynamics could not be resolved faithfully due to insufficient time coverage in the transient absorption experiment. Complementary TCSPC measurements are not precise enough to capture ultrafast dynamics

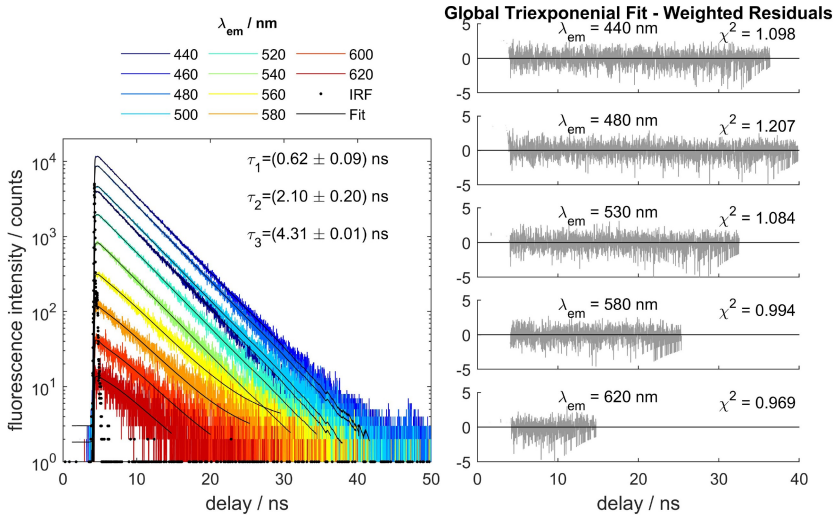

Figure 3. Exemplary TCSPC fluorescence decay traces of ROH in acetonitrile at the indicated wavelengths. The traces were globally fitted to three exponential functions (black solid lines) convoluted with the IRF (black dots). The right panels show exemplary the residual distributions for selected wavelengths with indication of the normalized χ^2 values.

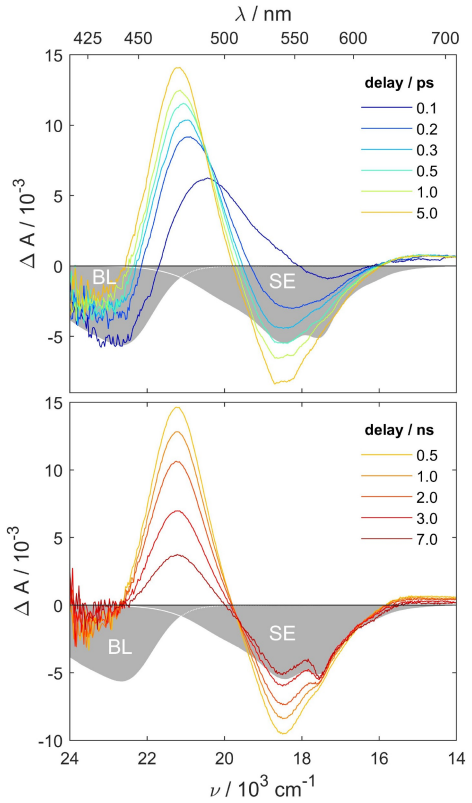

Figure 4. Femtosecond transient absorption spectra of the complex ROH:TOPO in acetonitrile (λ_{exc} = 410 nm). The upper panel shows the spectral evolution in the 5 ps time window at the delay times indicated in the legend. Later spectral changes are delayed until the ns time scale (lower panel). The gray-filled areas show normalized BL and SE bands obtained from the stationary absorption and fluorescence spectra of the ROH:TOPO complex in acetonitrile. See also Figure SI 3 for a spectral decomposition of the SE band.

but, in turn, expose undoubtedly slower irreversible dynamics involving the anionic species. This rules out *geminate* recombination in the excited state, the only protonation process conceivable at acid concentrations in the molar range. We discuss in the following global analysis addressing transient absorption and fluorescence time-resolved data to *model* reaction dynamics, extract *characteristic* rate constants and species-associated spectra of the molecular structures contributing to the proton-transfer reaction.

3. Discussion

Proton transfer dynamics of the ROH:TOPO complex was traced with TA measurements on the 10 ps, 1 ns and 8 ns time windows. The three datasets were analyzed globally with a three-exponential function, for which decay times are treated as global parameters and amplitudes are optimized locally. The resulting decay times τ_{1-3} are 0.82(1) ps, 31.5(2) ps and 4.93(3) ns (see Figure SI 8–12). A consecutive kinetic model was assumed and the Species-Associated-Difference-Spectra (SADS) were calculated analytically. The general procedure was previously described in Reference [24] and it is briefly sketched in the SI (section 1). The so-obtained SADS are shown in Figure 7 exemplary for two sets of data and in Figure SI 12 for all three datasets. Comparison with SE spectra extracted from steady-state fluorescence measurements, discloses the underlying reaction steps.

On a few picosecond timescale, a SE band rises around 540 nm (Figure 4, top panel). The ESA band peaking at about 475 nm at earliest time, blue shifts and rises in this time window too. This strong increase of ESA and SE signals cannot be due to a growing excited state population because it occurs much slower than the time duration of the excitation pulse (see Figure SI 2). Instead, spectral changes either affecting oscillator

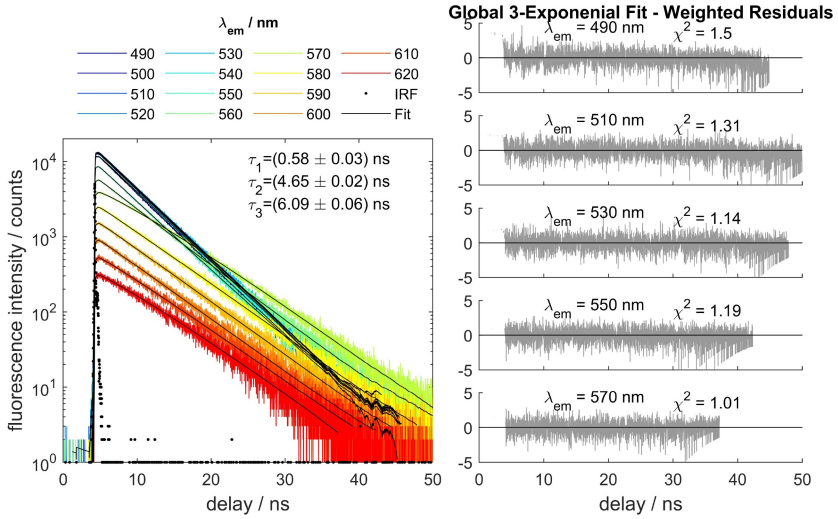

Figure 5. Time-resolved fluorescence decay of the ROH:TOPO complex measured at the indicated wavelengths in acetonitrile. The curves were fitted globally with a three-exponential function (black solid lines) convoluted with the instrument response function (IRF, black dots). The fitted decay times are shown in the inset. The panels on the right show the residuals distributions for some selected examples with indication of the normalized local χ^2 values corresponding to each wavelength.

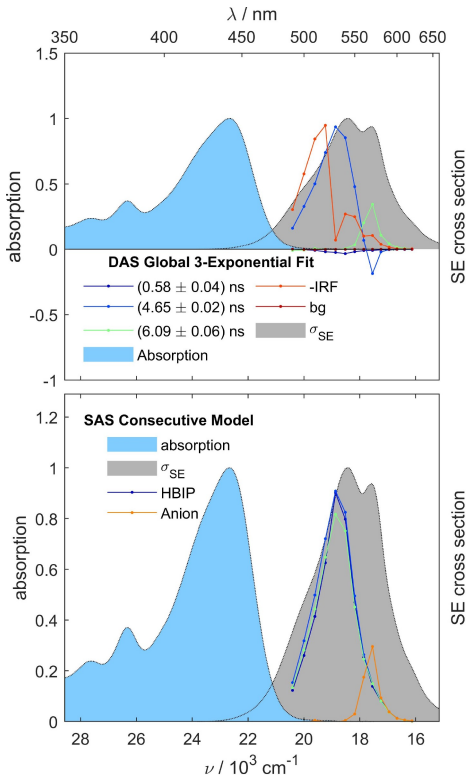

Figure 6. Spectral amplitudes of the exponential and impulsive contributions obtained in the three-exponential global fit of the time-resolved fluorescence, as indicated in the legend (top panel). Note that the impulsive contribution (IRF) was multiplied by −1. The background amplitude (bg) is also shown for completeness. The latter contributes negligibly and shows no spectral dependence. Steady-state absorption (cyan-filled curve) and SE (gray-filled curve) bandshapes are shown in the background for comparison. The DAS have been converted to cross-section of SE for consistency. The bottom panel shows the species-associated spectra (SAS) under the assumption of a consecutive kinetic model (see SI section 1 for details). Light blue, dark blue and light green spectra are assigned to the HBIP, which thus evolves in time in the nanosecond timescale. Note that the legend only refers to the dark blue spectrum for simplicity. Stationary absorption and SE bandshapes are shown as filled curves for comparison.

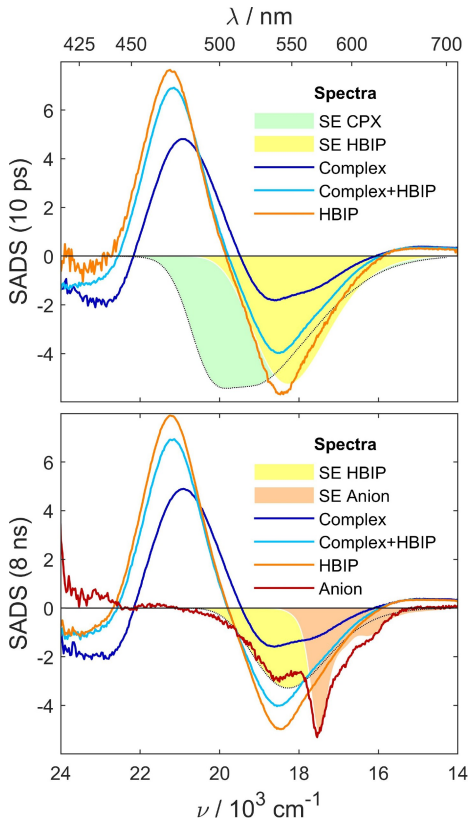

Figure 7. Species-Associated Difference Spectra (SADS) obtained from a global fit of three transient absorption datasets in the 10 ps, 1 ns (results not shown) and 8 ns timescales. The decay times were fitted as global parameters. The top frame shows the SADS for the measurements in the 10 ps timescale, scanned linearly with 20 fs steps. The bottom panel shows the SADS determined on the 8 ns timescale with logarithmic sampling of the pump-probe delay. Spectral assignment is indicated in the legend. Results for the 1 ns timescale are fully consistent with the data presented here (see Figure SI 12). Filled-spectra are SE bandshapes obtained from solvatochromic analysis of stationary fluorescence and are shown for comparison. The dotted lines trace the spectral flanks covered by overlapping spectra. See Reference [30] for further details.

strength or band overlap have to be invoked. Inspection of the SE bandshapes deduced for the complex and the HBIP suggests that the transformation of the complex into HBIP could be behind the observed behavior. Thus, decay of the complex SE (which bears negative sign and is shown as a green-filled bandshape in Figure 7) may at least qualitatively explain the rise of the ESA band and its blue shift. Concomitantly, rise of the HBIP SE band would naturally explain the increase of negative signal around 550 nm. A more quantitative analysis would demand knowledge about the spectral shape of the overlapping ESA band, which is not available. Despite, the process occurring with a time constant of 0.82(2) ps can be assigned to the intermolecular proton transfer reaction in the electronically-excited hydrogen-bonded complex. Since the spectral changes concentrate on the SE signals, while all other contributions remain essentially unaffected, proton transfer is most probably adiabatic, i.e. occurs on the same excited electronic surface.

Remarkably, the SE bandshapes shown in the top panel of Figure 7 were obtained by spectral decomposition and solvatochromic analysis of the stationary fluorescence spectra of the ROH:TOPO complex in an ample number of solvents.[30] This affords polarity-dependent SE spectra of complex and HBIP. The SE bandshapes match the positions of the SE bands in the TA spectra almost perfectly, which is taken as further confirmation of the solvatochromic analysis performed in our previous publication.[30]

The attention is now turned to the time-constant of the intermolecular proton transfer, $\tau_1 = 0.82(2)$ ps. The solvation response of acetonitrile was resolved by Ernsting and coworkers,[33] and was addressed later on in connection with intramolecular electron transfer.[34] These authors concluded a biphasic acetonitrile response with characteristic times of 70 fs and 0.60 ps, consistent with previous measurements.[35] Therefore, the close resemblance of the proton transfer rate constant and the slowest solvation component (0.82(2) ps versus 0.60 ps, respectively) indicates that the proton transfer reaction may

occur under solvent control.[21–23] Further, earliest contribution of the HBIP SE band would result from proton transfer during the ultrafast solvent relaxation component (60 fs), which remains unresolved in our experiment. In support, the spectral evolution of the transient absorption signal at delays when pump and probe pulses overlap is shown in Figure SI 13. These spectra show neither clear SE of the complex nor ESA at the leading edge of the pump pulse. Since SE must be present at earliest time after optical excitation via a dipole-allowed transition of the complex, one concludes that negative SE of the complex and positive ESA cancel out almost perfectly. As time increases, the ESA band develops and shows an earliest maximum at around 500 nm, suggesting that the underlying complex SE band decays. A red shifted SE band develops simultaneously at about 600 nm. Both bands continue to blue shift and grow as the pump pulse fades out. Thus, the spectral evolution resolved in the sub-picosecond timescale sets in at even faster timescales and is compatible with solvent controlled PT during the ultrafast component of solvent relaxation. While ultrafast stages of the process could not be time-resolved, observation of HBIP fluorescence at earliest time suggests that part of the ESPT reaction takes place on timescales compatible with the inertial part of the solvent relaxation function. Summarizing, intermolecular adiabatic proton transfer is demonstrated for the hydrogen-bonded ROH:TOPO complex and is consistent with ESPT occurring under solvent control.

Succeeding dynamics implies a further increase (10–20%) of the ESA and SE features of the transient spectrum. This occurs with a time constant τ_2 of 31.5(2) ps. The spectral evolution appears to be a continuation of the ultrafast stages analyzed above and is understood as an additional, slower transfer of population towards the HBIP configuration. It is however unclear at this stage which coordinate may explain this slower dynamics. Vibrational cooling is expected to occur after the PT reaction but the 31.5(2) ps time constant seems to be long for vibrational cooling.[36–38] Troe and co-workers reported a similarly high 20 ps cooling time constant for internal conversion of azulene in the halogenated solvent 1,1,2-trichloro-trifluoro-ethane,[39] suggesting that the halogenated alkyl side chains of ROH and TOPO decelerate to some extent energy transfer to the solvent. Alternatively, this time constant could result from reorientation of the hydrogen bond in complexes with unfavorable donor-acceptor (i.e. acid-base) geometries. However, it is conceivable that various unresolved processes hide behind this later small-amplitude stage for which a phenomeological time constant of 31.5(2) ps is deduced. Once this stage is completed, after *ca.* 50 ps delay, the spectrum stays practically constant until the nanosecond timescale, where signal decays and additional spectral changes are observed.

The global analysis on the 8 ns timescale reveals the increase of the characteristic SE of the anion with a time constant τ_3 of 4.93(3) ns. In this experiment, which scans delay times up to 8 ns, the contribution of the anion is obtained in a mixture with the HBIP, see lower panel of Figure 7. The later spectrum is resolved as a non-decaying component as the result of insufficient time coverage. To address this later stage of the process, picosecond-resolved fluorescence measurements were analyzed globally (see Figures 5 and 6). Remarkably, the fit shows main contributions for decay times of 4.65(2) and 6.09(6) ns. Two important observations are here underlined. First, the 4.65(2) ns component matches τ_3, the longest component detected in the TA experiment, while $\tau_4 = 6.09(6)$ ns mirrors the fluorescence decay time of the anionic form.[30] Second, the spectral amplitude associated to $\tau_4 = 6.09(6)$ ns in the time-resolved fluorescence matches the fluorescence spectrum of the anionic form too. Both observations confirm deprotonation of ROH in the ROH:TOPO complex, i.e. formation of the SSIP or FSIP in a process where no indication of geminate recombination could be found for the deprotonated form in the excited state.

We summarize the most important elements of the mechanism deduced up to now. Analysis of TA has demonstrated that, first, formation of the HBIP occurs in several stages extending from the femtosecond to 50 ps time window. During this full timescale no SE of the complex could be clearly detected because of the spectral overlap with the strong ESA band peaking at 470 nm at later times. Thus, it remains unclear whether complex SE disappeared completely in the 50 ps time window or some rest of it could still be hidden behind the strong ESA, as the shoulder of the SE spectrum at 475 nm suggests (Figure 6). Second, formation of the anion occurs in the nanosecond timescale with a time constant τ_3 of 4.93(3) ns. The decay of the anion population remains unresolved in the TA experiment, but time-resolved fluorescence indicates that it is formed with a time constant of 4.65(2) ns and decays with a time constant τ_4 of 6.09(6) ns. Formation and decay of RO^- are irreversible.

The analysis of the time-resolved fluorescence spectra is performed by spectral decomposition with the SAS deduced for the ROH, complex, HBIP and RO^- forms in reference [30]. Alternatively, a multiexponential fit might be used. Under the assumption of a consecutive kinetic model, the DAS would be converted into SAS (Figure 6). However, this latter method becomes unreliable in this case. It is affected by overlapping signals of the free ROH and the dissociating complex, which show comparable decay times and are thus very difficult to disentangle. This can be overcome by a time-dependent decomposition of the fluorescence spectra, from which time-dependent concentrations of all species are obtained, as it is discussed next (Figure 8). For this purpose, reconstructed fluorescence spectra were converted into SE cross-section and fitted at each delay time to a linear combination of the SE spectra of ROH, complex, HBIP and anion. The fits are excellent and answer the questions still open from the femtosecond TA analysis: a) unbound fluorescence of the ROH form is dominant below 480 nm and detectable up to at least 550 nm; b) fluorescence of the complex is non negligible in the nanosecond timescale and finally, c) complex and HBIP appear to be in constant ratio (Figure 9).

Time-dependent contributions to the TRES spectra were fitted to biexponential functions. Results are shown in Figure 9. The leading edge of the pump pulse is ignored

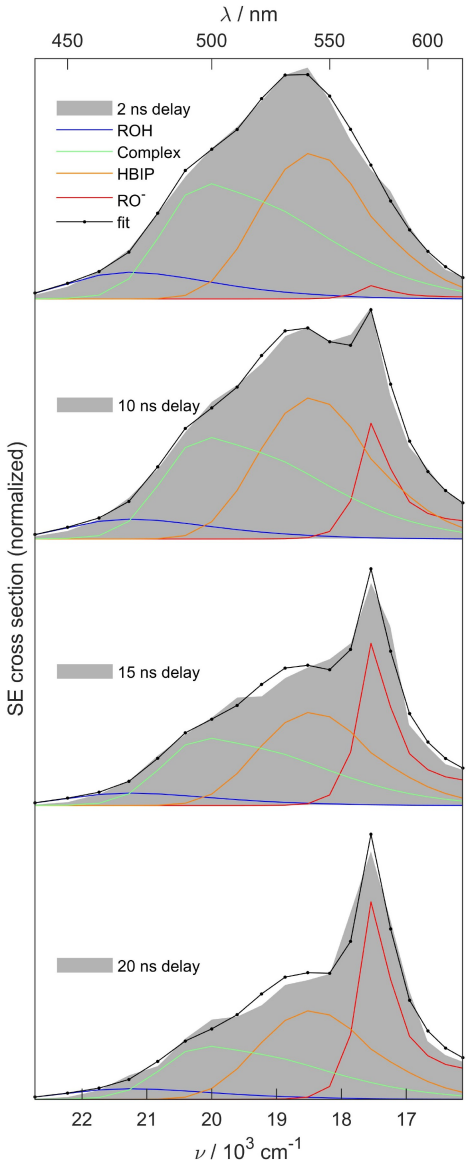

Figure 8. Spectral decomposition of the time-resolved fluorescence spectra, converted to SE cross section, as a linear combination of the basis spectra of the ROH, Complex, HBIP and RO^- forms. Delay times and contributions of the corresponding species are indicated in the legend.

since the fits are affected by the weak amplitude of the signal, the wavelength-dependent time-shift of the instrument response function and the use of SAS determined from stationary spectroscopy,[30] which may not be adequate for early times. The contribution of the anionic form evolves biexponentially with decay times of 4(2) ns and 7(4) ns. Note the much higher error in the decay time constants when fitting the contributions to the TRES data. Importantly, both exponential amplitudes are equal and bear opposite signs, confirming that the anion builds up in the excited state in an irreversible manner. The small negative dip at early times is seen as an artifact, due to minor shortcomings of the SAS for this timescale. HBIP evolves essentially monoexponentially with a time constant of 5(2) ns coincidental with the build-up time of the anionic form and thus demonstrating that the HBIP is the precursor of the anion. The ROH form evolves biexponentially too and the decay times of 3(2) ns and 4(2) ns. The latter and their associated amplitudes are somewhat coincidental with those deduced for ROH in pure acetonitrile (see Figure 3 and Figures SI 4 and 7), strongly suggesting that the dynamics of the ROH form is not affected by the presence of free TOPO, *i.e.* free ROH form contributes to the TRES data of the complex. Last, the complex contribution shows a biexponential evolution with decay times of 3(3) ns and 5(2) ns. The decay times are coincidental with those obtained for the ROH form, which can be taken as an indication of a reversible process connecting ROH and the complex. This is improbable: first, as already pointed out, the ROH form follows the same dynamics as already found in pure acetonitrile; second, if the complex would evolve biexponentially, much more involved dynamics should be observed for the PT reaction products HBIP and anion, contrary to observation. Therefore, we conclude that: a) complexation of free ROH in the excited-state lifetime can be excluded and b) the biexponential behavior suggested by the fit of the complex contribution in Figure 9 is an artifact resulting from the entanglement of complex and ROH form contributions, which overlap strongly spectrally and in time. Remarkably, the contributions of complex and HBIP are found to be in constant ratio already at the trailing edge of the 100 ps excitation pulse, indicating that an equilibrium between complex and HBIP is established. Assuming that the cross-sections for SE of complex and HBIP are approximately the same, an excited-state equilibrium constant $K_{PT} = \frac{[HBIP]}{[CPX]} \approx 1.2$ is estimated.

One last point to discuss is the fate of the anionic RO^- form and whether it is observed as SSIP or FSIP. The question can be answered semiquantitatively by analysis of TA data in the late nanosecond timescale. See Figure 10, where TA spectra averaged over 1 ns are shown. The transient spectrum at 100 ns delay shows the contribution of the ground-state anionic form, which remains long-living after deprotonation in the excited electronic state. It is expected that any RO^- in the form of SSIP immediately reprotonates in the ground state (on this timescale), so that long-living transient concentration of the ground state RO^- form is assigned to the FSIP. Consequently, the transient absorption at 100 ns delay would actually correspond to FSIP and is proportional to $\varepsilon_{RO^-} \cdot [RO^-] \cdot \Phi_{FSIP}$. Here, ε_{RO^-} is the molar absorption coefficient of RO^-, $[RO^-]$ is the molar concentration of RO^- reaching the ground state as result of the ESPT reaction, either as SSIP or FSIP, and Φ_{FSIP} is the quantum yield for the formation of the FSIP. Similarly, the transient absorption at 1 ns delay is assigned to the equilibrium distribution of CPX and HBIP forms in the excited state. Note that this delay is essentially prior to the ESPT reaction. Semiquantitatively, one may assume that the oscillator strength of $S_1 \rightarrow S_0$ SE is the same as that for $S_1 \leftarrow S_0$ absorption, for CPX and HBIP. Thus, the SE signal at 1 ns delay (Figure 10) is proportional to $\varepsilon_{CPX} \cdot ([CPX^*] + [HBIP^*])$. Note that ε_{CPX} corresponds to the ground-state absorption but it is assumed to be the same as that for SE in the S_1 state. Next, from the analysis of the linear

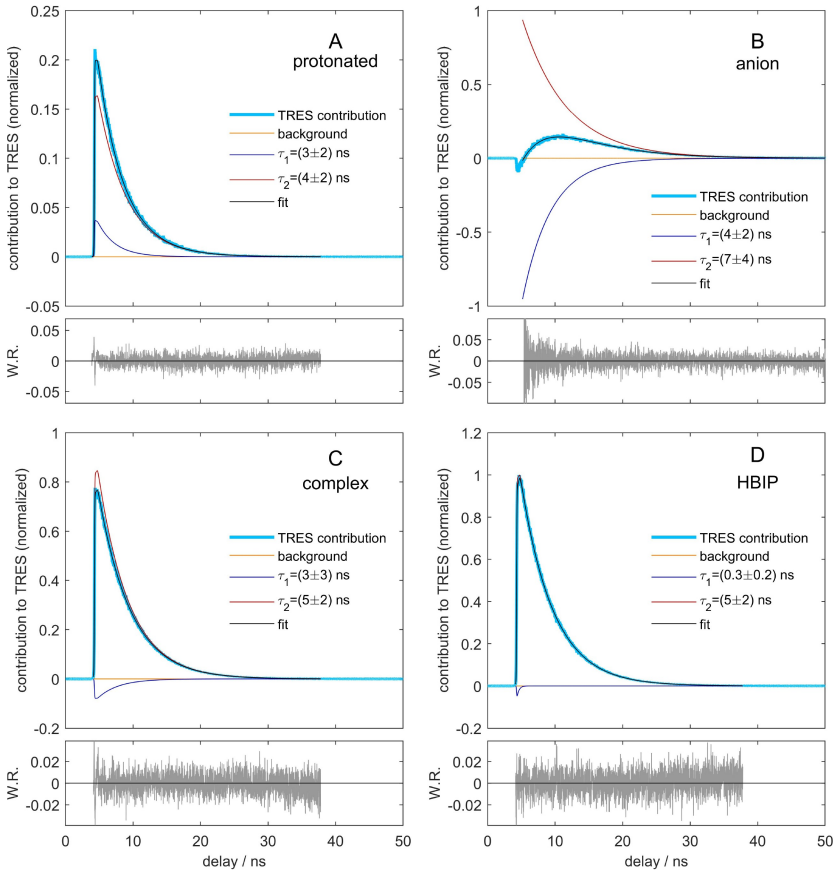

Figure 9. Biexponential fit of the contributions obtained by spectral decomposition of the time-resolved fluorescence spectra, as shown in Figure 8. The upper A–D panels show the contributions of each spectral species to the TRES data, the fits (black solid line) and the contributions of the exponentials and the background, as indicated in the legend. The distribution of weighted residuals is displayed underneath each one of the panels A–D. Spectral contributions were normalized by the maximum contribution of HBIP, which is the species contributing most to the time-resolved fluorescence spectra.

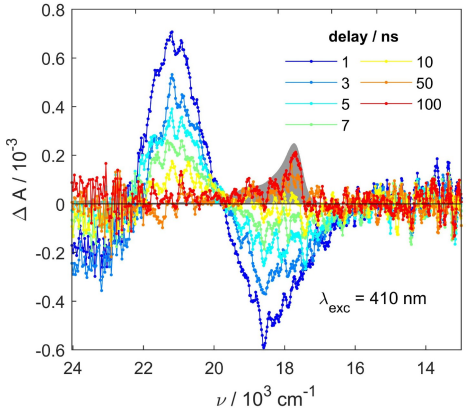

Figure 10. Transient absorption of complex in acetonitrile measured in the nanosecond timescale. Delay times are indicated in the legend. The stationary absorption spectrum of the deprotonated form is shown as a gray-filled curve. The excitation wavelength was tuned to 410 nm.

absorption spectra of the anion and the complex in the lowest energy absorption band, a ratio of maximal molar absorption coefficients of $\frac{\varepsilon_{RO^-}^{max}}{\varepsilon_{CPX}^{max}} = \frac{67\,240\ dm^3\ mol^{-1}\ cm^{-1}}{20\,530\ dm^3\ mol^{-1}\ cm^{-1}} \approx 3.3$ is deduced. Therefore, the ratio between the transient absorption at 564 nm and 100 ns delay and the SE signal at 540 nm and 1 ns delay reads $-\frac{\varepsilon_{RO^-}^{max}\cdot[RO^-]\cdot\Phi_{FSIP}}{\varepsilon_{CPX}^{max}\cdot([CPX^*]+[HBIP^*])}$. This quantity is approximately $\frac{0.2}{0.5}\pm 0.1$ (see Figure 10). Therefore, since the photodissociation quantum yield is found to be $\Phi_{diss} = \frac{[RO^-]}{[CPX^*]+[HBIP^*]} = 0.3 \pm 0.6$ (see Supporting Information, section 2), the TA ratio becomes $\frac{0.2}{0.5}\pm 0.1 = \frac{\varepsilon_{RO^-}^{max}}{\varepsilon_{CPX}^{max}}\cdot\frac{[RO^-]}{[CPX^*]+[HBIP^*]}\cdot\Phi_{FISP} \approx 3.3\cdot(0.3\pm0.6)\cdot\Phi_{FSIP}$. This leads to an estimated quantum yield for the formation of the excited-state FSIP of (0.4 ± 0.9). While this estimate is affected by large errors, the recapture of the proton by the left negative charge is consistent with previous findings in anti-bunching experiments in dimethylsulfoxide,[18] suggesting that solvent properties may not only affect the photodissociation rate, the composition of the ensuing complex/HBIP equilibrium but also the amount of free conjugated base formed too.

Once the behavior of the complex has been discussed, the time-resolved spectroscopy of the photoacid ROH in pure acetonitrile is briefly considered (Figures 2 and 3). The transient spectra evolve during the timescale of solvent relaxation, 1 ps. This evolution mirrors the one discussed for the ROH:TOPO complex: a SE band assigned to a ROH:

acetonitrile hydrogen-bonded complex develops at about 600 nm and the prominent ESA band first decays and then blue shifts in the 8 ps timescale. The spectrum remains essentially constant afterwards. In light of the discussion above, formation of the HBIP is deduced. The amplitude of the HBIP SE band is however much smaller than in the ROH:TOPO case and no indication of anion formation could be found. Therefore, proton transfer continues to occur under solvent control in pure acetonitrile but the complex/HBIP equilibrium is strongly shifted towards the complex side as consequence of the lower proton affinity of acetonitrile as complexation partner as compared to TOPO. This also prevents anion formation. Despite all efforts to reduce water content in acetonitrile, it remains open whether formation of HBIP in "pure" acetonitrile occurs via water traces in the solvent.

4. Conclusions

The photoinduced intermolecular proton transfer reaction in the photoacid-TOPO complex depicted in Scheme 2 was studied with the help of broadband femtosecond transient absorption and picosecond-resolved fluorescence at single wavelengths in acetonitrile. Results are interpreted with the help of global analysis and stimulated emission bandshapes isolated from stationary fluorescence spectra in a series of solvents.[30] The following picture emerges (Scheme 3): Photoexcitation of the complex triggers the proton transfer reaction, which occurs under solvent control in the sub-picosecond timescale. A quasi-equilibrium between the complex and the HBIP is established with an estimated constant K_{PT} of 1.2. This leads to the formation of the deprotonated form with a characteristic time constant of 4.65(2) ns. The latter is however the time constant accounting for the decay of the equilibrium populations of complex and HBIP. Under consideration of the equilibrium constant and the estimated decay times of both species, a microscopic time constant of about 13 ns for the dissociation of HBIP and the formation of RO^- is expected. The corresponding quantum yield is in the order of 30%. Finally, analysis of the long-living population of the anion form in the ground state suggests that about 40% of the anion molecules evolve towards the FSIP in the excited state. The majority of ion pairs seems to recombine.

This work discussed a set of experimental and analytical tools to address solvent effects on the dynamics of intermolecular proton transfer. The various stages of the intermolecular proton transfer reaction analyzed here extend from the femtosecond to the nanosecond timescale. Data interpretation is strongly hindered by the presence of free ROH form on the one hand, and by the spectral overlap of strong ESA and SE of the complex, on the other. Both factors prevent a complete elucidation of the ROH:TOPO decay dynamics and quantification of the complex/HBIP equilibrium populations. This also affects quantification of the quantum yield for the formation of the SSIP and thus the assessment of the quantum yield for the formation of the FSIP. Therefore, further experiments should aim to a better photoselection of the complex and higher spectro-temporal resolution with precise broadband fluorescence as the method of choice. In spite of those limitations, the equilibrium between the complex and HBIP is demonstrated. The latter is established within a few picoseconds and decays in the nanosecond timescale. This opens a broad time window to address the molecular structure of both intermediates with the help of vibrational spectroscopy, in particular, to understand whether proton's wavefunction shows bound or delocalized character.

To close, this work highlights the various levels at which solvent properties affect intermolecular proton transfer. They control the rate at which intrinsic proton transfer of strong photoacids takes place. They also influence the equilibrium populations of the complex and the HBIP, the dissociation of the HBIP to generate the SSIP and the escape probability of the conjugated acid to form the FSIP. All these effects condition the overall quantum yield of the proton transfer reaction.

Experimental Section

Sample Preparation. The photoacid tris-(2′,2′,2′-trifluoroethyl)-8-hydroxypyrene-1,3,6-trisulfonate (ROH) was prepared starting from 8-hydroxypyrene-1,3,6-trisulfonate (HPTS) as described in Reference [31]. Acetonitrile (Acros Organics, 99.9% extra-dry, water content $\leq$0.001%), trifluoroacetic acid (TFA, Sigma-Aldrich, $\geq$99% anhydrous, water content $\leq$0.05%) and tri-n-octylphosphine oxide (TOPO, Acros Organics, 99%) were used as received. Further purification of acetonitrile or handling under inert gas atmosphere showed no difference in the absorption and fluorescence spectra. The water content in the solutions here investigated is estimated to be at most 0.6 μM as deduced from the detection limit of the used Karl-Fischer titration.

For the steady-state spectra, solutions with 3 μM of photoacid ROH in extra-dry acetonitrile were prepared. Additionally, 30 mM TOPO were added for the complex solutions to ensure a complexation of the photoacid $\geq$97%.[30] To compensate for water impurities and to shift the ground state equilibrium of the photoacid to the ROH form, 300 μM TFA were added to the

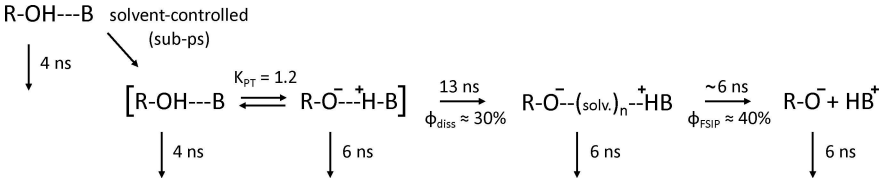

Scheme 3. Mechanism proposed for the photodissociation reaction of the ROH:TOPO complex in acetonitrile. Estimated time constants, excited-state equilibrium constant and quantum yields are indicated.

extra-dry acetonitrile. As shown before, trifluoroacetate does not serve as an ligand in polar solvents.[30] The solutions for the time-resolved fluorescence spectra and transient absorption measurements were prepared analogous but with a dye concentration of 18 μM and 300 μM, respectively. Optical spectra of the deprotonated form RO^- were determined in a ROH solution of non-dried acetonitrile (Fisher-Scientific, 99.9%).

Stationary Optical Spectroscopy. UV-Vis absorption spectra were measured with a Jasco V 650 spectrometer. A Jasco FP 6500 spectrofluorometer was used to obtain the fluorescence spectra. The latter were corrected for experimental factors with the function supplied by the manufacturer. The correction function was specifically tailored to our fluorometer.

Time-resolved fluorescence. Time-resolved fluorescence measurements were performed by the time-correlated single-photon counting (TCSPC) technique in an Edinburgh Instruments LifeSpec II system with 375 nm excitation (EPL-375), right angle geometry and at magic-angle polarization. Emitted fluorescence is spectrally selected with a double subtractive spectrometer and detected with a MCP-PMT. The instrument response function (FWHM) is about 100 ps broad, from which a time-resolution of 10 to 20 ps is estimated after deconvolution. 1 cm-thick quartz cuvettes (Starna) were used.

Femtosecond Broadband Transient Absorption Spectroscopy. Transient absorption measurements were performed in a 2 mm-thick quartz cells (Starna) and under continuous stirring. Optical excitation was performed with a tunable ≈100 fs laser pulse delivered by a commercial parametric amplifier (TOPAS Prime, Light Conversion), which was pumped with the fundamental of a Ti:Sa amplified laser system (Coherent Astrella F-5K). Transient absorption was measured with the Helios spectrograph (Ultrafast Systems) for parallel, perpendicular and magic angle pump-probe polarizations. The information was used to double-check complexation of ROH and TOPO: the rotational diffusion time obtained in anisotropy measurements increases from 62 ps in ROH to 121 ps in ROH:TOPO, indicating a larger hydrodynamic volume for the complex (Figure SI 15).[30] For the nanosecond to microsecond timescale, the EOS Spectrograph (Ultrafast Systems) was used. We provide here only a brief account of the main experimental parameters. A thorough description is given in Reference [40]. The excitation pulse was tuned to 410 nm for the photoacid and the complex. Typically, 100 nJ to 250 nJ pump energies were employed with pump spot sizes on the order of 250 μm from which fluences on the range of 2×10^{-4} J cm^{-2} result. A white-light continuum was generated on a sapphire substrate and used as probe. Data registration is performed at 4 kHz repetition rate with independent signal and reference spectrographs. Pump-probe time delays were varied with a high-speed computer-controlled linear translation stage (Thorlabs DDS300) combined with reflective optics for path multiplication. The average pump-probe cross-correlation amounts to 100 fs in this experiment. Spectra were corrected for the chirp of the white-light continuum.

Acknowledgments

The authors thank Prof. Dr. Karsten Heyne (Institut für Experimentelle Physik, Freie Universität Berlin, Germany), Prof. Dr. Marcus Motzkus (deceased on January 5, 2020) and Dr. Tiago Buckup (both at Physikalisch-Chemisches Institut, Universität Heidelberg, Germany) for support at the various stages of the project. This work was financed via the project JU650/8-1 and the Collaborative Research Center SFB 1078 (Project B7) of the Deutsche Forschungsgemeinschaft (DFG). We thank Viktoria Kiefer (Universität des Saarlandes, Germany) and Prof. Dr. Manuel Mosquera (Universidade de Santiago de Compostela, Spain) for a critical reading of the manuscript. Open Access funding enabled and organized by Projekt DEAL.

Conflict of Interest

The authors declare no conflict of interest.

Keywords: Eigen-Weller model · excited states · proton transfer · solvent relaxation · transient absorption spectroscopy

[1] K. Weber, *Z. Phys. Chem.* **1931**, *15*, 18–44.
[2] T. Förster, *Z. Elektrochem.* **1950**, *54*, 42–46.
[3] M. Eigen, *Angew. Chem. Int. Ed.* **1964**, *3*(1), 1–19.
[4] A. Weller, *Z. Elektrochem.* **1952**, *56*, 662–668.
[5] A. Weller, *Z. Elektrochem.* **1954**, *58*, 849–853.
[6] A. Weller, *Z. Phys. Chem. (Muenchen Ger.)* **1958**, *17*, 224–245.
[7] A. Weller, *Progress in Reaction Kinetics.* Pergamon Press, London, **1961**.
[8] M. Rini, B.-Z. Magnes, E. Pines, E. T. J. Nibbering, *Science* **2003**, *301*, 349–352.
[9] M. Rini, D. Pines, B.-Z. Magnes, E. Pines, E. T. J. Nibbering, *J. Chem. Phys.* **2004**, *121*(19), 9593–9610.
[10] O. F. Mohammed, D. Pines, J. Dreyer, E. Pines, E. T. J. Nibbering, *Science* **2005**, *310*(5745), 83–86.
[11] D. B. Spry, A. Goun, M. D. Fayer, *J. Phys. Chem. A* **2007**, *111*(2), 230–237.
[12] W. Liu, F. Han, C. Smith, C. Fang, *J. Phys. Chem. B* **2012**, *116*(35), 10535–10550.
[13] F. Han, W. Liu, C. Fang, *Chem. Phys.* **2013**, *422*, 204–219.
[14] P. Verma, A. Rosspeintner, B. Dereka, E. Vauthey, T. Kumpulainen, *Chem. Sci.* **2020**, *11*(30), 7963–7971.
[15] E. Pines, D. Huppert, N. Agmon, *J. Chem. Phys.* **1988**, *88*(9), 5620–5630.
[16] R. Gepshtein, P. Leiderman, L. Genosar, D. Huppert, *J. Phys. Chem. A* **2005**, *109*(42), 9674–9684.
[17] P. Leiderman, L. Genosar, D. Huppert, *J. Phys. Chem. A* **2005**, *109*(27), 5965–5977.
[18] M. Vester, A. Grueter, B. Finkler, R. Becker, G. Jung, *Phys. Chem. Chem. Phys.* **2016**, *18*, 10281–10288.
[19] T. Kumpulainen, B. H. Bakker, A. M. Brouwer, *Phys. Chem. Chem. Phys.* **2015**, *17*(32), 20715–20724.
[20] T. Kumpulainen, A. M. Brouwer, *Phys. Chem. Chem. Phys.* **2012**, *14*(37), 13019–13026.
[21] J. L. Pérez-Lustres, F. Rodriguez-Prieto, M. Mosquera, T. A. Senyushkina, N. P. Ernsting, S. A. Kovalenko, *J. Am. Chem. Soc.* **2007**, *129*(17), 5408–5418.
[22] M. Veiga-Gutierrez, A. Brenlla, C. C. Blanco, B. Fernandez, S. A. Kovalenko, F. Rodriguez-Prieto, M. Mosquera, J. L. Pérez-Lustres, *J. Phys. Chem. B* **2013**, *117*(45), 14065–14078.
[23] T. Kumpulainen, A. Rosspeintner, B. Dereka, E. Vauthey, *J. Phys. Chem. Lett.* **2017**, *8*, 4516–4521.
[24] A. Brenlla, M. Veiga Gutiérrez, M. C. Ríos Rodríguez, F. Rodríguez-Prieto, M. Mosquera, J. L. Pérez Lustres, *J. Phys. Chem. Lett.* **2014**, *5*(6), 989–994.
[25] Z. Qu, P. Li, X. Zhang, E. Wang, Y. Wang, P. Zhou, *J. Lumin.* **2016**, *177*, 197–203.
[26] J. C. Penedo, M. Mosquera, F. Rodriguez-Prieto, *J. Phys. Chem. A* **2000**, *104*(32), 7429–7441.
[27] L. Biczók, P. Valat, V. Wintgens, *Photochem. Photobiol. Sci.* **2003**, *2*(3), 230–235.
[28] Y. M. Lee, S.-Y. Park, H. Kim, T. G. Kim, O.-H. Kwon, *Methods Appl. Fluoresc.* **2016**, *4*(2), 24004.
[29] P. Verma, A. Rosspeintner, T. Kumpulainen, *RSC Adv.* **2020**, *10*, 23682–23689.
[30] A. Grandjean, J. L. Pérez Lustres, S. Muth, D. Maus, G. Jung, *J. Phys. Chem. Lett.* **2021**, *12*(6), 1683–1689.
[31] B. Finkler, C. Spies, M. Vester, F. Walte, K. Omlor, I. Riemann, M. Zimmer, F. Stracke, M. Gerhards, G. Jung, *Photochem. Photobiol. Sci.* **2014**, *13*(3), 548–562.

[32] J. B. Birks, *Photophysics of aromatic molecules / John B. Birks*. Wiley monographs in chemical physics. Wiley, London, 1970.
[33] J. Ruthmann, S. A. Kovalenko, N. P. Ernsting, D. Ouw, *J. Chem. Phys.* **1998**, *109*(13), 5466–5468.
[34] S. A. Kovalenko, J. L. Pérez Lustres, N. P. Ernsting, W. Rettig, *J. Phys. Chem. A* **2003**, *107*(48), 10228–10232.
[35] M. L. Horng, J. A. Gardecki, A. Papazyan, M. Maroncelli, *J. Phys. Chem.* **1995**, *99*(48), 17311–17337.
[36] S. A. Kovalenko, R. Schanz, V. M. Farztdinov, H. Hennig, N. P. Ernsting, *Chem. Phys. Lett.* **2000**, *323*(3-4), 312–322.
[37] V. M. Farztdinov, R. Schanz, S. A. Kovalenko, N. P. Ernsting, *J. Phys. Chem. A* **2000**, *104*(49), 11486–11496.
[38] P. Hamm, S. M. Ohline, W. Zinth, *J. Chem. Phys.* **1997**, *106*(2), 519–529.
[39] D. Schwarzer, C. Hanisch, P. Kutne, J. Troe, *J. Phys. Chem. A* **2002**, *106*(35), 8019–8028.
[40] N. Alagna, J. L. P. Lustres, N. Wollscheid, Q. Q. Luo, J. Han, A. Dreuw, F. L. Geyer, V. Brosius, U. H. F. Bunz, T. Buckup, M. Motzkus, *J. Phys. Chem. B* **2019**, *123*(50), 10780–10793.

Manuscript received: August 20, 2021
Revised manuscript received: September 28, 2021
Accepted manuscript online: September 29, 2021
Version of record online: November 8, 2021